Design, Simulations and Tests of a Novel Force and Moments Sensor for Instrumented Knee Implants

Pierre Gasnier, Jean-Yves Burlet, Ramzy Rammouz, Saifeddine Aloui, Sébastien Brulais, Guillaume Nonglaton, Liz Leconte, Francois Boux de Casson, Guillaume Dardenne, Eric Stindel

Design, Simulations and Tests of a Novel Force and Moments Sensor for Instrumented Knee Implants

Pierre Gasnier, Jean-Yves Burlet, Ramzy Rammouz, Saifeddine Aloui, Sébastien Brulais, Guillaume Nonglaton, Liz Leconte, François Boux de Casson, Guillaume Dardenne and Eric Stindel

***Abstract*— *Objectives:* Early identification of mechanical complications of total knee arthroplasties is of great importance to minimize the complexity and iatrogenicity of revision surgeries. There is therefore a critical need to use smart knee implants during intra or postoperative phases. Nevertheless, these devices are absent from commercialized orthopaedic implants, mainly due to their manufacturing complexity. We report the design, simulations and tests of a force and moments sensor integrated inside the tibial tray of a knee implant. *Methods:* By means of a "tray-pillar-membrane" arrangement, strain gauges and metal additive technology, our device facilitates the manufacturing and assembly steps of the complete system. We used finite element simulations to optimize the sensor and we compared the simulation results to mechanical measurements performed on a real instrumented tibial tray. *Results:* With a low power acquisition electronics, the measurements corroborate with simulations for low vertical input forces. Additionally, we performed ISO fatigue testings and high force measurements, with a good agreement compared to simulations but high non-linearities for positions far from the tray centre. In order to estimate the center of pressure coordinates and the normal force applied on the tray, we also implemented a small-size artificial neural network. *Conclusion:* This work shows that relevant mechanical components acting on a tibial tray of a knee implant can be measured in an easy to assemble, leak-proof and mechanically robust design while offering relevant data usable by clinicians during the surgical or rehabilitation procedures. *Significance:* This work contributes to increase the technological readiness of smart orthopaedic implants.**

Manuscript received in February, 2023. This work benefited funding from the French government via the national research agency as part of the Investments for the Future Programs, under the reference ANR-17-RHUS-0005 (FollowKnee Project).

P. Gasnier, J-Y Burlet, S.Aloui, S. Brulais, are with the System Department of CEA-Leti, 17 rue des martyrs, 38054 Grenoble, FRANCE (e-mail: pierre.gasnier@cea.fr).

R. Rammouz was with CEA-Leti and is now with IMEC, Kapeldreef 75, 3001 Leuven, BELGIUM (e-mail: ramzy.rammouz@imec.be).

G. Nonglaton is with the Health Department of CEA-Leti, 17 rue des martyrs, 38054 Grenoble, FRANCE (e-mail: guillaume.nonglaton@cea.fr).

L. Leconte is with SLS France, 32 Bd de la Haie des Cognets, 35136 Saint-Jacques-de-la-Lande (e-mail: liz.leconte@sls-france.fr).

F. Boux de Casson was with Stryker is now with BLUE ORTHO, 22 chemin du Vieux Chêne, 38240 Meylan, FRANCE (e-mail: francois.bouxdecasson@blue-ortho.com.)

G. Dardenne is with LATIM, 12 Av. Foch, 29200 Brest, FRANCE (e-mail: guillaume.dardenne@univ-brest.fr).

E. Stindel is with University of Western Brittany Brest - UBO, 3 Rue des Archives, 29238 Brest, FRANCE (e-mail: eric.stindel@chu-brest.fr).

***Index Terms*— Total Knee Arthroplasty, instrumented knee implants, tibial tray, tibial prosthesis**

I. Introduction

OVER the past decade, the number of Total Knee Arthroplasty (TKA) has doubled in developed countries and could quadruple by 2030 [1], [2]. This expansion is essentially due to the ageing of the population, the increase in obesity, but above all by the increasingly broadened indications towards young patients with less advanced arthrosis. Globally, a considerably larger increase of TKA among individuals younger than 65 years, but highly functionally demanding (*e.g.* running or playing golf), compared to the other age groups is observed worldwide [3]. However, the surgical operations carried out at an early stage can lead to more complications that often require revision surgery [4]. In addition, these repeated surgeries are also more expensive, more iatrogenic and require more rigorous medical monitoring [5]. The primary reasons for revision arthroplasty are infection, instability, pain, and aseptic loosening. This is why an optimal surgical procedure, followed by early identification of postoperative complications [6], particularly those of a mechanical nature such as instability, malalignment, bearing surface wear, unbalanced knee, and tibial insert dissociation, would significantly reduce the need for revisions [7], [8]. Although the relationship between post-TKA kinematics and postoperative complications like aseptic loosening is still an ongoing subject, there is a strong interest for the evaluation of the knee joint contact forces and moments after TKA to assess surgical outcomes [9], [10]. For example, the knee adduction and flexion moments are important parameters to quantify the prosthesis loading and could help recognizing abnormalities in gait pattern to determine adequate rehabilitation strategies [11]. This is the reason why many works [12]–[15] have shown their interest in measuring the femoral contact forces and moments or the location of the Center of Pressure (CoP) acting on the tibial component of knee implants, not only for preclinical testing of implants but also during the intraoperative and postoperative phases.

For over twenty-five years, an important part of the research works has concentrated on the tibial part of knee implants more than on distal femoral replacements [16]. Two types of devices have been studied: i) disposable instrumented tibial inserts mainly used in intra-operative contexts and ii) tibial

trays mainly used for the postoperative phase. Our work aims to address the intraoperative and postoperative phases with an instrumented tibial tray.

On one side, the clinical benefit of intraoperative disposable instrumented inserts has already been proven for sensor-assisted TKA. Indeed, it has been shown [17], [18] that evaluating the knee joint pressure distribution intraoperatively is helpful for orthopedic surgeons to fine-tune the implant positioning and the soft tissue balancing. As an example, the VERASENSE (OrthoSensor, Inc.), provides numerical values of the medial and lateral compartmental loads [17]. For its part, the device of [19] is composed of two sensitive plates (one for each condyle) containing three deformable bridges instrumented with thick-film piezoresistive sensors. The device measures the reaction forces amplitude and estimates the location of the applied loads. Nevertheless, those devices are dedicated to intraoperative phases and therefore do not face the same implantability constraints and mechanical robustness as long-term implantable medical devices.

In the field of tibial trays, one of the first measurement concepts was patented in 1993 [20], published in 1996 [21] and later by the research team of D'Lima and Colwell [22], [23]. The research team carried out the first *in vivo* implantation of a wireless instrumented tibial implant in 2004 [13], [24]. The sensing elements are located in the anteromedial, anterolateral, posteromedial and posterolateral quadrants, inside the tibial tray. The mechanism of transduction is based on posts deforming four membranes in flexion above which strain gauges are located. Even though this transducer provides both the magnitude and the location of the CoP, the four membranes deform only in the z direction. Consequently, only the z component of the force is obtained and the devices could only give an approximate evaluation of the varus–valgus and flexion-extension moments. Moreover, this tray-centered integration solution results in i) a thicker tray than a standard knee prosthesis and ii) a more complex assembly due to the fact that the gauges are not directly accessible from the stem where the acquisition electronics is often housed which complicates the assembly of the overall system. In 2006, D'Lima and Colwell's research team [12], [14] proposed another design principle to measure three forces and three moments from the femur to the tibia. This stem-centered solution was later taken up by the team led by Bergmann and its colleagues [15] and is based on a "stem-in-stem" design which facilitates the connection to the electronics. The femoral loads on the proximal plate are transferred to a vertical inner stem inside which semiconductor gauges are glued. Although this concept enables the measurement of six load components, the inner and outer stems must be welded together [15] or assembled using a complex thermal shrink-fit process [12] and the gauges are glued to the inner wall of the stem. Even though this contribution was essential for the knowledge of *in vivo* knee loading [25], [26], the above mentioned concept seems complicated and expensive to manufacture and assemble in a mass market context, limiting its use to biomedical studies rather than rehabilitation phases. Other interesting attempts should also be mentioned : in 2011, [27], [28] proposed a tibial component equipped with four piezoelectric elements located in the four tibial quadrants, to quantitatively evaluate the ligamentous balance. However, beyond its complexity of integration, the ageing and brittleness of piezoelectric elements when subjected to shocks still need to be studied, particularly in the context of the knee joint. More recently, [29] repurposed a commercially available tire pressure sensor with the aim of reducing the space allocated to the sensors. Unfortunately, the capacitive pressure transducer, initially dedicated to air pressure measurements, must be coupled to several mechanical interfaces to adapt the high mechanical input force to a micrometer-level deformation. While this contribution is interesting for its multisensor aspect, the current prototype only allows for the measurement of a single compressive load, and no proposals for fully integrating this concept have been made at this time. It should also be mentioned that all those long-terms implanted devices are facing energy supply constraints, which are often addressed with wireless power transmission technologies, and particularly with inductive coupling techniques [30].

Factually, despite the latest advances on the market for instrumented knee implants [31], forces and moments measurements or magnitude and location of the CoP remain absent in commercialized orthopaedic implants. From these observations, arises two research questions :

- Can forces and moments measurements be achieved through a leak-proof and easy to assemble knee implant design facilitating the installation of the sensing elements and their connections to the acquisition electronics?
- How the above mentioned measurements can be converted into values meaningful for clinicians, like the CoP applied by the femoral condyles on the tibial tray?

Our work addresses these questions by proposing a novel way to integrate force and moments measurements and validates its assumptions through finite element simulations corroborated by experimental results on a custom-made instrumented knee implant. We should mention that the proposed sensor is part of a more comprehensive system that also includes a tibiofemoral angle measurement using accelerometers and an infection detection using pH and temperature sensors. The entire system is powered by a RFID-based inductive coupling technology. Section II explains the proposed measurement concept adapted to a knee implant and the simulation method used to design the sensor. Section III details the fabrication, assembly and measurement results of the prototype. In this section, a machine learning method is also proposed to evaluate the CoP coordinates and the normal force applied on the tibial tray from the raw values of the sensor. Section IV provides an interpretation of the results and a discussion on the relevance of such an approach.

II. Materials and Methods

A. Measurement concept

The proposed measurement concept is inspired from the "boss–diaphragm structure" initially made in Silicon microfabrication technology [32] and applied for biomedical applications [33], [34]. This MEMS sensor consists of a suspended and therefore deformable membrane, which has a rigid pillar

in its center ensuring the transmission and the amplification of the forces by means of a lever arm effect. Those sensors are placed on the back side of the membrane and are mounted in a double Wheatstone Bridge (WB). When a force is applied on the pillar, the piezoresistors are then longitudinally compressed or elongated which electrically unbalances the midpoints of the WBs. Fig. 1 shows a simulation example of the longitudinal strain in the x direction for an transverse force $F_z = 180\,\mathrm{N}$ applied at the center (see section II-C). It also depicts the electrical connection and placement of the double WB at the back side of the membrane as well as the gauges' state of strain in this case.

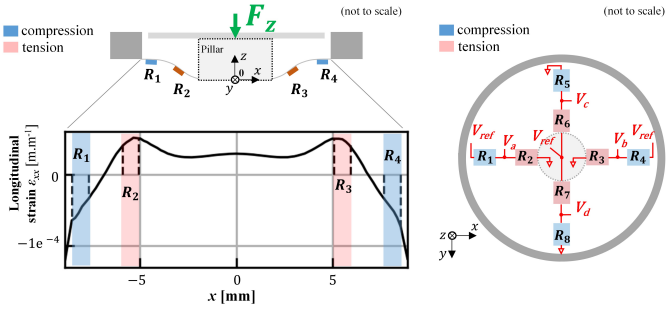

(a) (b)

Fig. 1: a) FEM modeling showing the longitudinal strain of $R_{1,2,3,4}$ for $F_z = 180\,\mathrm{N}$ on the proposed sensor design (see section II-C) and b) drawings of the boss–diaphragm structure (bottom view) in the same force case.

For each strain gauge, let δ_i denote the relative variation of its nominal resistance R_i such as $\delta_i = \frac{\Delta R_i}{R_i}$ and neglect the errors due to the transverse sensitivity in the gauges. For a strain gauge aligned with the x axis (*i.e.* $R_{1,2,3,4}$), δ_i is then related to the longitudinal strain ε_{xx} by (1):

$$\delta_i = K\varepsilon_{xx} \tag{1}$$

with K the axial factor of the gauge.

On the electrical side, the voltages V_a, V_b, V_c and V_d referred to the ground (see Fig. 1b), are related to each longitudinal strains δ_i based on the WB configuration:

$$\begin{aligned} V_a &= \frac{1+\delta_2}{2+\delta_1+\delta_2}V_{ref} \\ V_b &= \frac{1+\delta_3}{2+\delta_3+\delta_4}V_{ref} \\ V_c &= \frac{1+\delta_5}{2+\delta_5+\delta_6}V_{ref} \\ V_d &= \frac{1+\delta_8}{2+\delta_7+\delta_8}V_{ref} \end{aligned} \tag{2}$$

From [34], [35], V_a, V_b, V_c and V_d can be combined to measure the transverse force (F_z) and two shear components of the force (F_x and F_y) applied on the pillar, by means of U_z, U_x and U_y given in (3):

$$\begin{aligned} U_x &= V_b - V_a \\ U_y &= V_d - V_c \\ U_z &= (V_a + V_b) - (V_c + V_d) \end{aligned} \tag{3}$$

Replacing V_a, V_b, V_c and V_d in (3) by their expressions and simplifying second-order terms gives:

$$\begin{aligned} U_x &\approx \frac{1}{4}(\delta_6 + \delta_8 - \delta_7 - \delta_5)V_{ref} \\ U_y &\approx \frac{1}{4}(\delta_1 + \delta_3 - \delta_2 - \delta_4)V_{ref} \\ U_z &\approx \frac{1}{4}(\delta_7 + \delta_3 + \delta_6 + \delta_2 - \delta_4 - \delta_5 - \delta_1 - \delta_8)V_{ref} \end{aligned} \tag{4}$$

In the case of a transverse force applied at the center (case of Fig. 1), it can be shown that the positive strains (tension) are equals $\delta_2 = \delta_3 = \delta_6 = \delta_7 = \delta$ and opposites of the negative strains (compression) $\delta_1 = \delta_4 = \delta_5 = \delta_8 = -\delta$. Then, equation (4) simplifies to :

$$\begin{aligned} U_x &\approx 0 \\ U_y &\approx 0 \\ U_z &\approx 2\delta \times V_{ref} \end{aligned} \tag{5}$$

Then, U_z varies proportionally with the strain δ due to the applied transverse force F_z while U_x, U_y are approximately equal to zero. The same method can by used to measure the two shear forces F_x and F_y applied on the pillar along x or y respectively, through the measurement of U_x and U_y respectively. For example, if a force were applied on the pillar along the x direction only, *i.e.* a shear force F_x creating a moment about the y axis, $R_{2,4}$ would be longitudinally compressed and $R_{1,3}$ would be elongated, whereas $R_{5,6,7,8}$ would not be compressed nor elongated. This specific case would result in $U_z = U_y = 0$ and in U_x proportional to F_x. The boss-diaphragm structure thus makes it possible to measure the shear (along x and y) and the transverse (along z direction) components of a point load applied on the pillar.

B. Application to knee implants

We redesigned and optimized the above-mentioned measurement concept regarding the size and the materials constraints of a the tibial tray of a knee implant. For that purpose, the sensor is composed of a proximal plate receiving the forces of the femoral condyles (through the polyethylene insert), linked by a circular pillar to a distal plate resting on the medial and lateral condyles of the tibia. Instead of piezoresistors, the WB is composed of eight foil strain gauges which are glued to the back side of the membrane as depicted in Fig. 2. This "tray-pillar-membrane" type arrangement enables to measure the components F_z (vertical component of the force), M_x and M_y (moments about this x and y axis respectively) applied on the tibial tray. For comparison, a rather similar arrangement was proposed by [21] inside the tibial tray with the difference that the four membranes only deform in the z direction, which does not allow a direct measurement of the moments.

Compared to the state of art, this arrangement offers two advantages : i) The eight gauges are located on a flat and easily accessible surface preferably in the same compartment as the acquisition electronics underneath, which considerably facilitates the assembly of the complete system. ii) We use 3D printing technology to fabricate the proximal plate, the

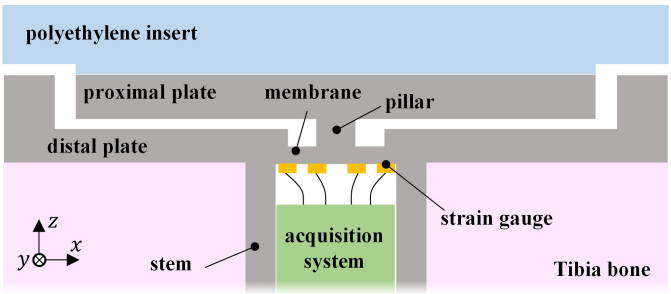

Fig. 2: Cross section of the proposed "tray-pillar-membrane" arrangement in the frontal plane (schematics principle not to scale)

pilar and the distal plate within the same element which also facilitates the assembly. It also helps to provide an hermetic packaging which is required to protect the implant's electronic circuitry and sensors from the harsh environment of the human body.

To assess the measurement performance of the proposed concept in a real situation, we proposed a knee implant design in collaboration with clinicians and orthopedic surgeons involved in the Followknee project [36]. Fig. 3 shows the 3D model and parameters of the proposed instrumented tibial knee implant. The mediolateral (ML) width L_{ML} of the implant and the anteroposterior (AP) length L_{AP} of the implant correspond to the average dimensions of one of the smallest tibial tray available on the market prostheses.

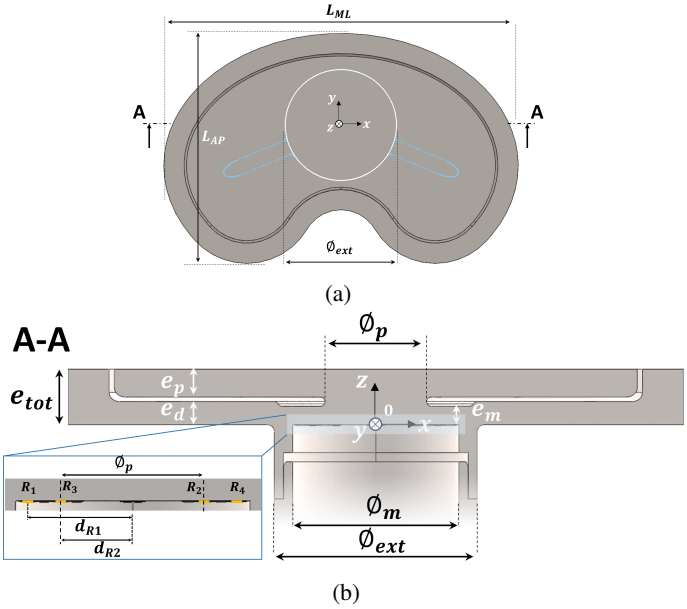

(a) (b)

Fig. 3: 3D model and parameters of the proposed instrumented knee implant

Due to the design's complexity and its asymmetry, we performed Finite Elements (FE) simulations of the instrumented knee implant which are detailed in section II-C.

C. Simulation

Having set the overall parameters of the knee implant design with clinicians, the appropriate geometric parameters of the sensor part (membrane, pillar) were optimized by static analysis with FE simulations in COMSOL Multiphysics. Table I gives the parameters used for the simulations. Specific foil strain gauges from Hottinger Bruel & Kjaer have been selected for reasons of low power consumption thanks to their high nominal resistance value ($R_0 = 1\,\mathrm{k}\Omega$) and compactness. The area of the gauges's carrier is indeed $2.54\,\mathrm{mm} \times 2.16\,\mathrm{mm}$, making them compatible with the inner diameter of the stem. For a fixed membrane size, the gauges placement on the membrane was determined according to i) the overall gauge dimensions, set by the carrier's dimensions to avoid overlapping and ii) the region which maximizes the stress in the gauge's measuring grid in order to optimize the sensitivity of the sensor. The sensitivity appeared to be optimal when the gauges $R_{1,4,5,8}$ and $R_{2,3,6,7}$ are placed as close as possible to the inner surface of the stem and at the pillar level respectively.

TABLE I: Parameters used for the design and simulation of the instrumented knee implant

Symbol	Value	Parameter
L_{ML}	70 mm	Medio-Lateral width of the implant
L_{AP}	46 mm	Antero-posterior length of the implant
ϕ_{ext}	22 mm	Outer diameter of the stem at the level of the tray
ϕ_p	12 mm	Diameter of the pillar
ϕ_m	18 mm	Diameter of the membrane
e_d	2.5 mm	Thickness of the distal plate
e_p	3 mm	Thickness of the proximal plate
e_m	2 mm	Thickness of the membrane
e_{tot}	6 mm	Total thickness tibial tray
d_{R1}	8 mm	Distance of $R_{1,4,5,8}$'s centers (measuring grids) to the membrane's center
d_{R2}	5.5 mm	Distance of $R_{2,3,6,7}$'s centers (measuring grids) to the membrane's center
S_{car}	2.54 mm× 2.16 mm	Area of the gauge's carrier
S_{grid}	1.57 mm× 0.79 mm	Area of the gauge's measuring grid
K	1.97	Axial factor of the gauge
Y_{TI}	110 GPa	Young's modulus of the material (Ti)

We ran numerous static analyses with 10 transverse loads F_z in 20 N increments up to 180 N for each of the 11 chosen positions on the tibial tray of the implant. The loads were applied on a $\varnothing 4\,\mathrm{mm}$ circle. A fixed constraint was set on the entire bottom area of the distal plate, simulating a perfect anchoring of the knee implant inside the tibia bone. For each position and loads values, the uni-axial components of the strain tensor ε_{xx} and ε_{yy} on the entire membrane surface were computed. Fig. 4 shows an example of a simulation result in the case of a 180 N load applied at the $(0, 0)$ coordinate of the tray. In Fig. 5, the same load is applied at the $(0, 20)$ coordinate. Fig. 4 and Fig. 5 also shows the ε_{xx} and ε_{yy} on the "x line" (*i.e.* for $y = 0$) and "y line" (*i.e.* for $x = 0$) respectively.

For each simulation run (*i.e.* for each coordinate and load), the mean strains ε_{xx} and ε_{yy} of each gauge were computed. The WB's voltages $V_{a,b,c,d}$ were then calculated from (2) and finally U_x, U_y, U_z are worked out from (3). For the sake of paper clarity, the simulation results are exposed in section III and compared with their corresponding measurement results on two different test benches.

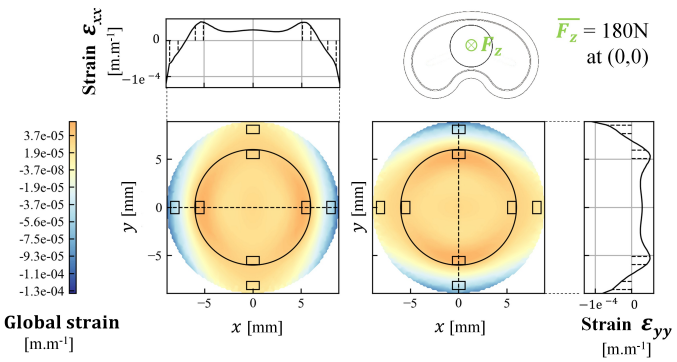

Fig. 4: Simulated uni-axial strains ε_{xx} and ε_{yy} on the back side of the membrane for F_z =180 N applied at $(0, 0)$

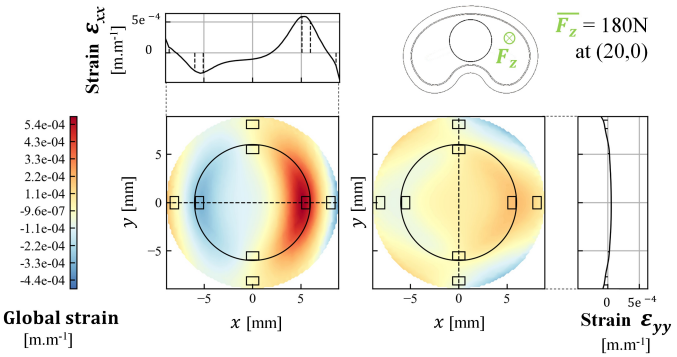

Fig. 5: Simulated uni-axial strains ε_{xx} and ε_{yy} on the back-side of the membrane for F_z =180 N applied at $(20, 0)$

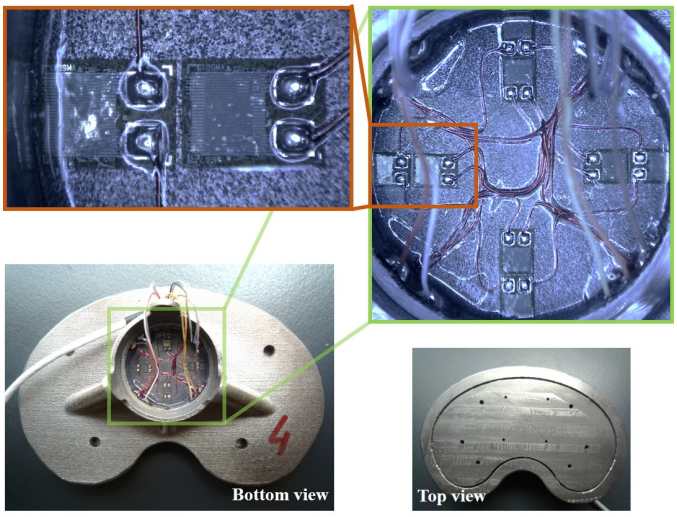

Fig. 6: Pictures of an assembled tibial tray (bottom-left/right), showing zooms on the membrane (top-right) and on the R_1 and R_2 gauges (top-left)

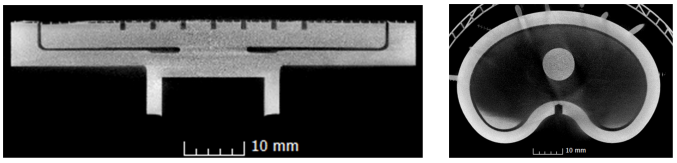

(a) (b)

Fig. 7: X-ray tomography of the prototype : cuts in the (a) coronal plane and in the (b) transverse plane

D. Assembly and fabrication

The tibial tray (proximal and distal plates, pillar) has been manufactured by Selective Laser Melting technology at SLS France with an industrial metal 3D printing machine (SLM125, SLM solution) with a titanium alloy (Ti6Al4V ELI powder, Grade 23) proposing a 20 µm resolution. The prototype was then machined (5 Axis CNC) to reduce the tray and membrane's thicknesses and improve their roughness. The strain gauges were then installed on the back-side of the membrane at the specified location by Hottinger Bruel & Kjaer. Fig. 6 shows an assembled prototype with a focus on the membrane.

A X-ray tomography was used to check the structural integrity of the additively manufactured tibial tray before the CNC machining step and the membrane's surface finish. The cut in the coronal plane (Fig. 7a) shows relatively accurate dimensional build, but the tomography resolution (45 µm) was not sufficient to detect possible porosity (which may be between 1 and 20 µm with the SLM used). Nevertheless, Fig. 7a highlights a slight subsidence of the proximal plate at its tip which is particularly noticeable in the transverse cut (Fig. 7b) on the bottom-left. These defects will have an impact on the measurements performance for high input forces as detailed afterwards.

III. Results

A. Experimental test bench

1) Electronic acquisition system: The acquisition system used to measure the differential voltages of the WBs is shown in Fig. 8a. Targeting a smart orthopedic implant, we proposed a low power and small size electronics architecture which is moreover compatible with a RFID system as a wireless power transfer strategy. For the sake of paper compacity, the integration developments and the means of power supplying of the electronics are not described here. As shown in Fig. 8a, it is based on a 24-bit, delta-sigma analog-to-digital converter from Texas Instrument (ADS124S08) interfaced with the SPI peripheral of a microcontroller (STM32L4A6) set at a data rate of 100 samples per seconds. These two components were chosen for their compromise between performance, small size (QFN type packages) and low power consumption in order to integrate the electronics in the stem right below the membrane. The WBs are duty-cycled by means of two NMOS transistors driven by periodic pulses. This pulsed mode enables the WBs to conduct only during the analog-to-digital conversion (*i.e.* a few milliseconds), thus reducing the power consumption of the acquisition system (P_{mean} = 4.5 mW at 3.3 V). The complete acquisition system fits on a 370 mm^2 PCB surface which is compatible with the integration constraints of the stem.

2) Mechanical test benches: We used two mechanical test benches, a low-force test bench and a high-force test bench. The low-force mechanical test-bench (Fig. 8b) is a custom made CNC machine comprising a software-controlled motorized frame moving in the x, y and z directions with a 100 µm accuracy and applying compression up to 180 N to the prototype. The ⌀4 mm finger is coupled to a load cell (Interface SML-220N) having a non-linearity under 0.05 %FS.

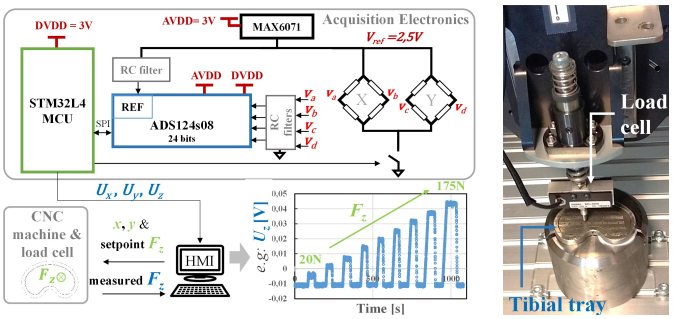

(a) (b)

Fig. 8: a) Schematic of the acquisition system compliant with integration requirements and b) pictures of the low-force mechanical test bench

In the same way as FE simulations, several loads in 20 N increments were applied vertically on the tray during 20 s for 11 locations. At the same time, the differential voltages U_x, U_y, U_z were datalogged from the acquisition system and the real force F_z applied by the bench was measured. The localized load method and the maximum range were determined by the test bench capacity and the maximum load it can withstand. A high-force test bench, not allowing an automated and precise positioning of the load, has also been used to verify the relevance of the proposed concept for force amplitudes closer to a human joint (see section III-C).

B. Simulation vs measurements : low-force test bench

The low-force test bench applied ten vertical load values ranging from 0 to 180 N at each of the 11 positions of the proximal plate (the same positions as the simulations). For the measured values, the offsets were nulled when no strain is applied as if the bridges were balanced. Fig. 9, Fig. 10 and Fig. 11 show the simulated and experimental voltages of the WBs as a function of the forces and the resultant moments. Concerning the measured voltage values, it should be noted that for each position, the entire temporal acquisitions comprising the 10 successive loads are displayed on the graphs hence superimposing the measurements at each steady state load values.

We used standard linear regression techniques to evaluate the force sensitivity S_{Fz} and moment S_{Mx} and S_{My}. A coefficient of determination greater than 0.99 was observed for all coordinates both on simulations and measurements. In Table II, one can also note a rather good agreement between the simulated and measured sensitivities. The average measured sensitivities are -2.79×10^{-4} mV/N.mm, -3.03×10^{-4} mV/N.mm and 2.76×10^{-3} mV/N for S_{Mx}, S_{My} and S_{Fz} respectively. The observed differences are discussed in Section IV.

C. Simulation vs measurements : high-force test bench

To verify the relevance of the proposed concept for force amplitudes closer to a human joint, another mechanical test bench was used. For that purpose, the high-force test bench shown in Fig. 12a uses a twin-column compression tester

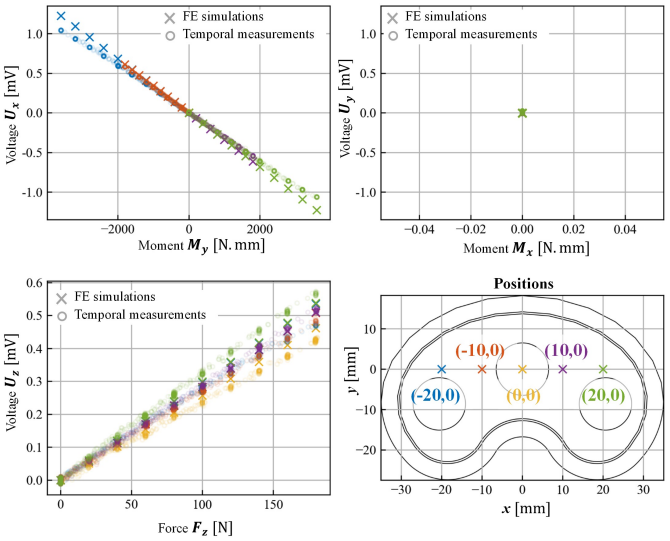

Fig. 9: Voltages U_x, U_y, U_z from FE simulation (crosses) and measurement (circles) for 5 different application points (ML positions).

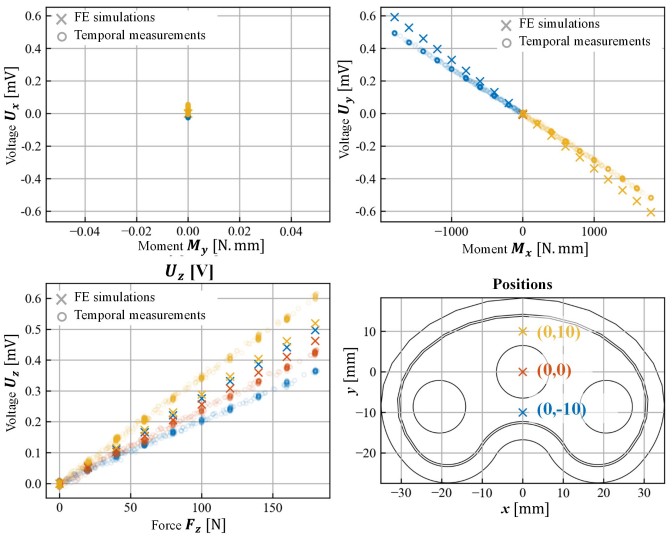

Fig. 10: Voltages U_x, U_y, U_z from FE simulation (crosses) and measurement (circles) for 3 different application points (AP positions).

(Mecmesin MultiTest-25i) with a ILC-s 5000N loadcell and the same $\varnothing 4$ mm finger as the above mentioned measurement results. Vertical loads were applied up to 4.9 kN at the $(0, 0)$, $(-20.6, -8.6)$ and $(20.6, -8.6)$ coordinates while monitoring the test-bench input force. Using linear regression techniques on U_z, a coefficient of determination of 0.85 has been observed on both simulation and measurements. We chose those coordinates according to the location of the femoral condyles globally encountered on this implant size. Fig. 13 shows the results for an input force ramp up to 2.6 kN, highlighting a probable contact point between the proximal and distal plates for F_z loads above 70 N and 110 N for the $(-20.6, -8.6)$ and $(20.6, -8.6)$ coordinates respectively. This aspect is discussed in section IV.

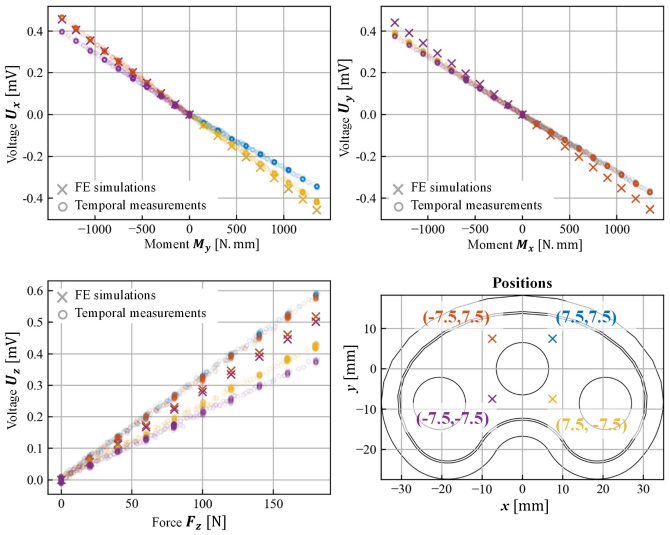

Fig. 11: Voltages U_x, U_y, U_z from FE simulation (crosses) and measurement (circles) for 4 different application points (AM, AL, PM, PL positions)

TABLE II: Force and moments sensibilities : measurements vs FE simulations

Coordinates (x, y)	**Sensitivity** S_{Mx} [mV/N.mm] (error* vs FEM)	**Sensitivity** S_{My} [mV/N.mm] (error* vs FEM)	**Sensitivity** S_{Fz} [mV/N] (error* vs FEM)
(0,0)	-	-	2.36×10^{-3} (-8.2%)
(-20,0)	-	-2.96×10^{-4} (-13.2%)	2.73×10^{-3} (-8.1%)
(-10,0)	-	-3.23×10^{-4} (-5.0%)	2.71×10^{-3} (-3.9%)
(10,0)	-	-3.02×10^{-4} (-11.2%)	2.87×10^{-3} (1.4%)
(20,0)	-	-3.04×10^{-4} (-10.9%)	3.22×10^{-3} (7.7%)
(0,10)	-2.86×10^{-4} (-14.9%)	-	3.40×10^{-3} (18.1%)
(0,-10)	-2.73×10^{-4} (-17.3%)	-	2.04×10^{-3} (-26.1%)
(7.5,7.5)	-2.74×10^{-4} (-18.5%)	-2.55×10^{-4} (-24.6%)	3.29×10^{-3} (14.2%)
(-7.5,7.5)	-2.74×10^{-4} (-18.5%)	-3.41×10^{-4} (-1.2%)	3.24×10^{-3} (12.5%)
(7.5,-7.5)	-2.97×10^{-4} (-12.0)	-3.11×10^{-4} (-7.7%)	2.38×10^{-3} (-14.7%)
(-7.5,-7.5)	-2.78×10^{-4} (-14.7%)	-2.92×10^{-4} (-13.4%)	2.13×10^{-3} (-23.7%)

* relative error : $(S_{meas} - S_{fem})/S_{fem}$

D. Fatigue testings

To integrate the acquisition electronics inside the whole knee implant, a leak proof biocompatible casing must be proposed. For that purpose, the tibial baseplate was assembled with a 3D printed stem (Ti6Al4V ELI powder, 2 mm wall thickness) by laser welding. To prove the mechanical robustness of the assembly (baseplate and stem), fatigue testings were performed at a subcontractor according to the ISO 14879-1 standard [37] (see Fig. 12b). Five million cycles were applied on the medial side at a frequency of 13 Hz with a sinusoidal load from 90 N to 900 N at coordinate $(11.4, 23.3)$. A 13 mm diameter, 6 mm thick ultra-high-molecular-weight polyethylene spacer was used between the load and the tibial baseplate. This assembly passed the tests successfully and showed no defect.

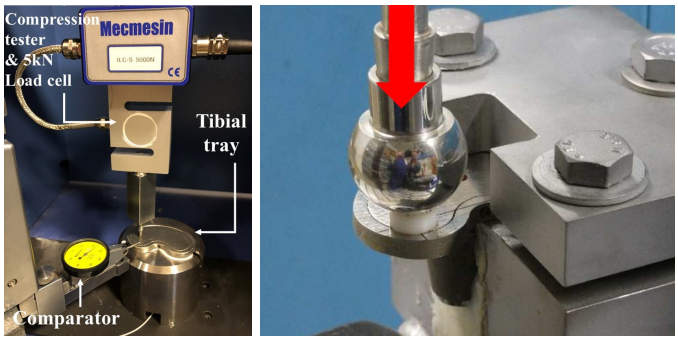

(a) (b)

Fig. 12: a) High-force test bench (up to 5 kN) and b) Fatigue test bench of the proposed instrumented knee implant (without electronics) according to the ISO 14879-1 standard.

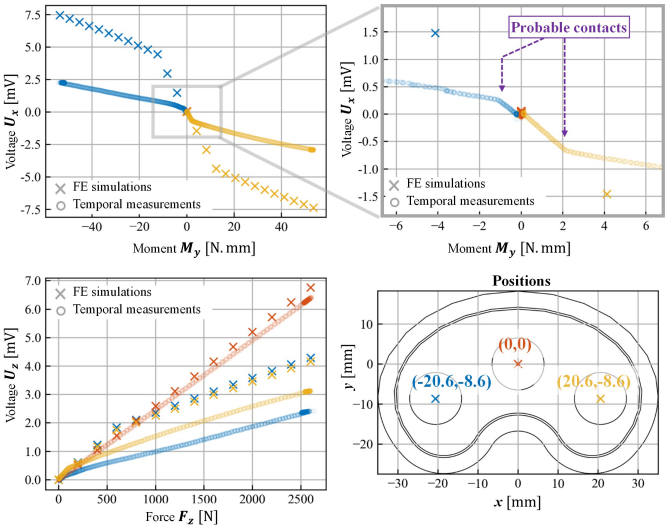

Fig. 13: voltages U_x, U_y, U_z from FE simulation (crosses) and measurement (circles) for 3 different application points and a force ramp up to 2.6 kN (high-force test bench, see Fig. 12a).

E. From voltages measurements to data usable by clinicians

The final objective of this work is to show that the proposed solution allows to estimate the CoP coordinates (X_{CoP}, Y_{CoP}) as well as the normal force F_z applied on the proximal plate of the tibial tray. This problem can be addressed using machine learning and Artificial Neural Networks (ANNs) in particular, as there are some imperfections in the system, non-linearities and noise in the transfer function that makes learning more suitable over a complex analytic solution. ANNs [38] are generic function approximation tools that have been used in a variety of signal processing fields. They rely on a set of data points (inputs and outputs) measured on a specific system in order to approximate the function that transforms the inputs to the outputs. It has been shown [39] that, given a sufficient amount of data, ANNs can learn to approximate any continuous function provided it has sufficient number of

neurons as well as a non-linear activation. We defined the CoP as the weighted center of the pressure on a given surface. We also neglected tangent forces and focused on estimating only the force component F_z normal to the tibial tray surface. We used 14192 data points of the setup detailed in section III-A.2, *i.e.* 11 known positions and 9 F_z values ranging from 0 to 180 N for each position. A data point corresponds to a group of six values (U_x,U_y, U_z, x, y and F_z) sampled simultaneously. For this particular data set, 50% of the data points were used as a training (80%) / validation (20%) set and 50% were used as a test set. The data was preprocessed by applying a min/max scaler on both inputs and outputs which accelerates convergence time and stabilizes the learning process. We used a feed forward network with a short cut from the output of the first layer to the input of the last layer, inspired by [40] with a rectified linear unit activation function on the six first layers as shown in Fig. 14. This network is small enough to be implemented on an embedded microcontroller-based system.

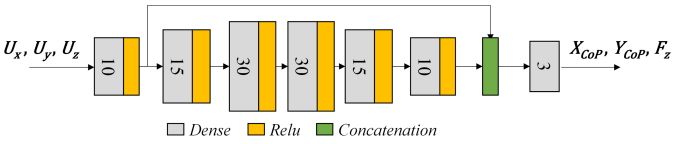

Fig. 14: Neural Network Architecture

After learning for 500 epochs on the training data, *i.e.* 500 cycles through the full training data set, with early stopping on the validation data, the ANN was able to determine both the CoP as well as the value of F_z. Fig. 15 shows a comparison between the true and the predicted CoP coordinates and F_z values for nine force levels and for the 10 successive test positions. This figure also shows a zoom on X_{CoP} for $F_z = 160\,\mathrm{N}$ and $180\,\mathrm{N}$ applied at $(7.5, -7.5)$. On this specific test set, the root mean squared (RMS) error is around $0.4\,\mathrm{mm}$ and $0.3\,\mathrm{mm}$ (RMS distance error of $0.7\,\mathrm{mm}$ from (0,0)) for X_{CoP}, X_{CoP} respectively and $1.7\,\mathrm{N}$ for F_z, with maximum absolute errors ranging from $2.3\,\mathrm{mm}$ and $1.5\,\mathrm{mm}$ for the positions (distance error of $2.7\,\mathrm{mm}$ from (0,0)) and $7.2\,\mathrm{N}$ respectively. We also observed that the position estimation error is higher for positions farther from the center of the tray.

IV. Discussion

For low input forces (up to 180 N), there is a rather good agreement between the FE simulations and the raw measurements with mean absolute errors on sensitivities equal to 16%, 11% and 12.6% for S_{Mx}, S_{My} and S_{Fz} respectively. These results are encouraging in view of the potential significant differences between the simulations and the imperfect manufactured and assembled prototype. However, the prototype shows notable imperfections : for the same absolute distance from the tray center, it was observed a stronger variation of the force sensitivities. This is particularly noticeable for AP loads (*e.g.* (0,10) vs (0,-10)), see Fig. 10) than for ML loads (*e.g.* (10,0) vs (-10,0), see Fig. 9). Indeed, the sensitivity for an anterior load is 67% higher than that of the same posterior load at ($\pm$ 10,0) whereas it is 6% higher for a medial load compared with the same lateral load at $(0, \pm 10)$. This effect, also visible in simulations to a lesser extent, is due to the

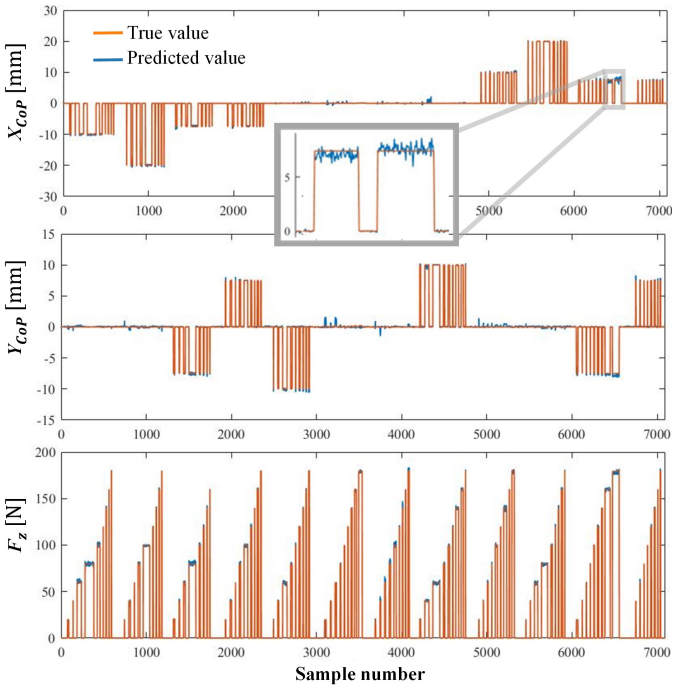

Fig. 15: Specific test set with a comparison between the true and estimated positions of the CoP (X_{CoP}, Y_{CoP}) as well as the normal force F_z for the 10 successive test positions.

non-symmetrical geometry of the implant along the x axis which changes the anchoring conditions of the x-axis gauges compared to the y-axis gauges.

The proposed concept was also tested at high input forces up to $4.9\,\mathrm{kN}$ without any deterioration. For a $2.3\,\mathrm{kN}$ ramp applied in the $(0, 0)$ position, the measurements are very close to FE simulations. As expected for high input forces applied far from the centre, the simulations predicted a mechanical contact between the proximal plate and the distal plate (from $600\,\mathrm{N}$) resulting in a high non-linearity (a sudden change in slope) of the response. Experimentally, this mechanical contact unfortunately happens at lower input force ($70\,\mathrm{N}$ and $100\,\mathrm{N}$ for the medial or lateral loads). This is probably due to the i) initial subsidence of the proximal plate and/or ii) a residue of powder between the proximal and distal plates at the end of the additive manufacturing process (see Fig. 7). The manufacturing process therefore needs to be improved in order to control the maximum displacement of the tray and the sensor's response on the complete input force range and all positions. The assembly imperfections, the non-symmetry of the mechanical design and the significant non-linearities of the prototype fully justify the use of ANNs to locate the CoP coordinates and the force F_z applied on the proximal plate.

We showed that, in spite of the non-linearity of the sensor particularly far from the tray center, it is possible to use an ANN-approach to counterbalance the sensor imperfections. This approach must nevertheless be validated on a larger number of devices and for other coordinates. However, we showed that an ANN used with a few but well chosen training points can be a simple solution to replace a long calibration phase. Even though the output of the ANN is satisfying, there are many optimizations that must be studied. As the neural

architecture is shallow and may be sub-optimal, the most impactful change would be to apply a more thorough hyper-parameters optimization of the ANN in order to increase the accuracy of the output estimation. In any case, this example shows that ANNs can be used to estimate the magnitude and the location of the CoP as function of the voltages provided by our sensor, with low amount of processing power and error. Concerning, the CoP and force estimation, it is nevertheless important to note the limitation of our study: the used ANN was not trained nor tested on high input forces. Efforts must be made to address this aspect in the future.

Compared to the sensor design presented in [15], our sensor is currently limited to measuring only one force component and two moment components. The absence of lateral and anterior force measurements is a limitation that could potentially be addressed by incorporating additional strain gauges at specific and dedicated positions. For our device, a solution must also be found to prevent the ingrowth of connective tissues between the distal and proximal tray that could potentially lead to measurement errors [41]. This could be achieved, for example, by using a plastic seal along the circumference of the proximal tray, similar to the approach taken by [15]. Another option could be to 3D print a proximal tray with a thin metal layer that closes the gap while still allowing for tray movement. But on an engineering aspect, we claim that the proposed concept could facilitate the assembly steps of such an instrumented implant compared to former works for two reasons. Firstly, thanks to the proposed design and the use of 3D printing technology, the proximal plate, the distal plate and possibly the stem can be manufactured in a single fabrication step within the same mechanical element. In addition, it should be noted that the strain sensors used in this study are affixed to a flat and easily accessible surface, making our proposed solution potentially compatible with a more simple and standard assembly process. For instance, a single pre-wired gauges block, similar to commercially available rosette-type elements, could embed the eight gauges and their output connections and be directly glued onto the membrane's surface, thereby simplifying the assembly step even more and reducing manufacturing variations. For the complete system's assembly, the stem underneath has an advantageous shape and volume to house the electronics and can be easily welded to build a leak-proof, biocompatible and mechanically robust casing. A welded assembly (tray and stem) was submitted to fatigue testings in accordance to the ISO 14879-1 and passed them successfully, with the aim of increasing the technological maturity of the proposed integration choices.

The current study has nevertheless certain limitations that should be highlighted. First, because the reported results reflect the performance of the proposed approach within the limitations of our test benches (low-force/high-precision and high-force/low-precision test benches), future endeavors should aim to expand the experimental scope of our study. This includes encompassing measurements with a wider range of forces with improved precision, to provide a more comprehensive understanding of the approach's capabilities and limitations. Another limitation of our validation method that deserves highlighting is that the implant was only tested under point load conditions (a $\varnothing 4\,\mathrm{mm}$ circle), without considering the application of distributed forces on the proximal plate. To assess the system's accuracy under more realistic loading scenarios, it is crucial to perform simulations and measurements in conditions closer to a knee joint, *i.e.* with i) a more representative load-bearing area of the condylar contacts, both in terms of location and contact areas and ii) by taking the polyethylene insert between the femoral and tibial elements into account. The impact of various factors, such as the size, shape, location, direction, and number of distributed loads applied on the proximal plate, will further validate the proposed concept for TKA applications. Finally, although our device has demonstrated the ability to measure forces and moments, it is important to acknowledge that its application in identifying post-TKA complications is not demonstrated in this paper. In future studies, we plan to conduct a study on cadaveric specimens with orthopedic surgeons, to evaluate those metrics accompanied by tibiofemoral angle measurements. It will allow us to further investigate this question before potential *in vivo* implantation and will potentially open up new possibilities for research. Regarding the financial and healthcare implications of the device for patients and healthcare systems, it is too early to quantify them. These aspects will need to be carefully examined, particularly with regards to the device's potential social impacts, such as its effect on patient outcomes, quality of life, healthcare costs, and accessibility to knee implant technology.

V. Conclusion

In this work, we proposed a novel way to integrate a force and moments sensor inside the tibial tray of a knee implant. The measurement concept and its integration were validated by means of FE simulations corroborated with experimental results on a dedicated tibial tray design validated by clinicians and orthopedic surgeons. The proposed integration facilitates the manufacturing and assembly steps of the complete sensor system, including its acquisition electronics. A small-size ANN trained with a few calibration points was used to estimate the magnitude and the location of the CoP as function of the three voltages provided by our sensor with fairly low amount of error. The ANN will also be able to compensate the sensor's non-linearities at high input forces. Since the key elements (gauges, membrane, pillar) of the sensor are positioned in the centre of tray, this concept allows to use the same sensor design inside various patient specific implant shapes and sizes. This would allow to combine the benefits of customized total knee replacement techniques and sensor functions for intraoperative and postoperative contexts, while offering an easy to manufacture smart knee implant. As a follow-up, it would be relevant to study the integration of this concept in other joint implants, like the hip or the shoulder joints.

Acknowledgment

The authors would like to thank Hottinger Bruel & Kjaer France for their help concerning the assembly of the sensor.

REFERENCES

[1] C. Pabinger, H. Lothaller, and A. Geissler, "Utilization rates of knee-arthroplasty in OECD countries," *Osteoarthritis and Cartilage*, vol. 23, no. 10, pp. 1664–1673, Oct. 2015.

[2] E. Losina, A. D. Paltiel, A. M. Weinstein, E. Yelin, D. J. Hunter, S. P. Chen, K. Klara, L. G. Suter, D. H. Solomon, S. A. Burbine, R. P. Walensky, and J. N. Katz, "Lifetime Medical Costs of Knee Osteoarthritis Management in the United States: Impact of Extending Indications for Total Knee Arthroplasty," *Arthritis Care & Research*, vol. 67, no. 2, pp. 203–215, 2015.

[3] M. Le Stum, T. Gicquel, G. Dardenne, M. Le Goff-Pronost, E. Stindel, and A. Clavé, "Total knee arthroplasty in France: Male-driven rise in procedures in 2009–2019 and projections for 2050," *Orthopaedics & Traumatology: Surgery & Research*, p. 103463, Oct. 2022.

[4] R. S. Charette, M. Sloan, R. D. DeAngelis, and G.-C. Lee, "Higher Rate of Early Revision Following Primary Total Knee Arthroplasty in Patients Under Age 55: A Cautionary Tale," *The Journal of Arthroplasty*, vol. 34, no. 12, pp. 2918–2924, Dec. 2019.

[5] D. J. Hunter and S. Bierma-Zeinstra, "Osteoarthritis," *The Lancet*, vol. 393, no. 10182, pp. 1745–1759, Apr. 2019.

[6] E. W. Paxton, O. Furnes, R. S. Namba, M. C. S. Inacio, A. M. Fenstad, and L. I. Havelin, "Comparison of the Norwegian Knee Arthroplasty Register and a United States Arthroplasty Registry," *JBJS*, vol. 93, no. Supplement_3, p. 20, Dec. 2011.

[7] K. Gustke, G. Golladay, M. Roche, G. Jerry, L. Elson, and C. Anderson, "Increased satisfaction after total knee replacement using sensor-guided technology," *Bone and Joint Journal*, vol. 96B, no. 10, pp. 1333–1338, 2014.

[8] M. L. Harris, P. Morberg, W. J. M. Bruce, and W. R. Walsh, "An improved method for measuring tibiofemoral contact areas in total knee arthroplasty: a comparison of K-scan sensor and Fuji film," *Journal of Biomechanics*, vol. 32, no. 9, pp. 951–958, Sep. 1999.

[9] A. Perillo-Marcone and M. Taylor, "Effect of Varus/Valgus Malalignment on Bone Strains in the Proximal Tibia After TKR: An Explicit Finite Element Study," *Journal of Biomechanical Engineering*, vol. 129, no. 1, pp. 1–11, Feb. 2007.

[10] M. Du, J. Sun, Y. Liu, Y. Wang, S. Yan, J. Zeng, and K. Zhang, "Tibio-Femoral Contact Force Distribution of Knee Before and After Total Knee Arthroplasty: Combined Finite Element and Gait Analysis," *Orthopaedic Surgery*, vol. 14, no. 8, pp. 1836–1845, 2022.

[11] G. L. Hatfield, C. L. Hubley-Kozey, J. L. Astephen Wilson, and M. J. Dunbar, "The Effect of Total Knee Arthroplasty on Knee Joint Kinematics and Kinetics During Gait," *The Journal of Arthroplasty*, vol. 26, no. 2, pp. 309–318, Feb. 2011.

[12] B. Kirking, J. Krevolin, C. Townsend, C. W. Colwell, and D. D. D'Lima, "A multiaxial force-sensing implantable tibial prosthesis," *Journal of Biomechanics*, vol. 39, no. 9, pp. 1744–1751, Jan. 2006.

[13] D. D. D'Lima, S. Patil, N. Steklov, J. E. Slamin, and C. W. Colwell, "Tibial Forces Measured In Vivo After Total Knee Arthroplasty," *The Journal of Arthroplasty*, vol. 21, no. 2, pp. 255–262, Feb. 2006.

[14] D. D. D'Lima, S. Patil, N. Steklov, S. Chien, and C. W. Colwell, "In vivo knee moments and shear after total knee arthroplasty," *Journal of Biomechanics*, vol. 40, pp. S11–S17, Jan. 2007.

[15] B. Heinlein, F. Graichen, A. Bender, A. Rohlmann, and G. Bergmann, "Design, calibration and pre-clinical testing of an instrumented tibial tray," *Journal of Biomechanics*, vol. 40, pp. S4–S10, Jan. 2007.

[16] S. J. G. Taylor and P. S. Walker, "Forces and moments telemetered from two distal femoral replacements during various activities," *Journal of Biomechanics*, vol. 34, no. 7, pp. 839–848, Jul. 2001.

[17] K. A. Gustke, G. J. Golladay, M. W. Roche, L. C. Elson, and C. R. Anderson, "A new method for defining balance: promising short-term clinical outcomes of sensor-guided TKA," *The Journal of Arthroplasty*, vol. 29, no. 5, pp. 955–960, May 2014.

[18] J. C. Chow and L. Breslauer, "The Use of Intraoperative Sensors Significantly Increases the Patient-Reported Rate of Improvement in Primary Total Knee Arthroplasty," *Orthopedics*, vol. 40, no. 4, pp. e648–e651, Jul. 2017.

[19] D. Crottet, T. Maeder, D. Fritschy, H. Bleuler, L. P. Nolte, and I. P. Pappas, "Development of a force amplitude- and location-sensing device designed to improve the ligament balancing procedure in TKA," *IEEE Transactions on Biomedical Engineering*, vol. 52, no. 9, pp. 1609–1611, Sep. 2005.

[20] N. Kovacevic, "Knee joint load measuring instrument and joint prosthesis," US Patent US5 197 488A, Mar., 1993.

[21] K. R. Kaufman, N. Kovacevic, S. E. Irby, and C. W. Colwell, "Instrumented implant for measuring tibiofemoral forces," *Journal of Biomechanics*, vol. 29, no. 5, pp. 667–671, May 1996.

[22] B. A. Morris, D. D. D'Lima, J. Slamin, N. Kovacevic, S. W. Arms, C. P. Townsend, and C. W. J. Colwell, "e-Knee: Evolution of the Electronic Knee Prosthesis : Telemetry Technology Development," *JBJS*, vol. 83, no. 2, p. S62, Oct. 2001.

[23] D. D. D'Lima, C. P. Townsend, S. W. Arms, B. A. Morris, and C. W. Colwell, "An implantable telemetry device to measure intra-articular tibial forces," *Journal of Biomechanics*, vol. 38, no. 2, pp. 299–304, Feb. 2005.

[24] D. D. D'Lima, S. Patil, N. Steklov, J. E. Slamin, and C. W. J. Colwell, "The Chitranjan Ranawat Award: In Vivo Knee Forces after Total Knee Arthroplasty," *Clinical Orthopaedics and Related Research®*, vol. 440, pp. 45–49, Nov. 2005.

[25] I. Kutzner, B. Heinlein, F. Graichen, A. Bender, A. Rohlmann, A. Halder, A. Beier, and G. Bergmann, "Loading of the knee joint during activities of daily living measured in vivo in five subjects," *Journal of Biomechanics*, vol. 43, no. 11, pp. 2164–2173, Aug. 2010.

[26] I. Kutzner, S. Küther, B. Heinlein, J. Dymke, A. Bender, A. M. Halder, and G. Bergmann, "The effect of valgus braces on medial compartment load of the knee joint – in vivo load measurements in three subjects," *Journal of Biomechanics*, vol. 44, no. 7, pp. 1354–1360, Apr. 2011.

[27] S. Almouahed, M. Gouriou, C. Hamitouche, E. Stindel, and C. Roux, "Design and Evaluation of Instrumented Smart Knee Implant," *IEEE Transactions on Biomedical Engineering*, vol. 58, no. 4, pp. 971–982, Apr. 2011.

[28] S. Almouahed, C. Hamitouche, and E. Stindel, "Optimized Prototype of Instrumented Knee Implant: Experimental Validation," *IRBM*, vol. 38, no. 5, pp. 250–255, Oct. 2017.

[29] W. D. Anderson, S. L. M. Wilson, and D. W. Holdsworth, "Development of a Wireless Telemetry Sensor Device to Measure Load and Deformation in Orthopaedic Applications," *Sensors*, vol. 20, no. 23, p. 6772, Jan. 2020.

[30] K. Agarwal, R. Jegadeesan, Y.-X. Guo, and N. V. Thakor, "Wireless Power Transfer Strategies for Implantable Bioelectronics," *IEEE Reviews in Biomedical Engineering*, vol. 10, pp. 136–161, 2017.

[31] F. Cushner, P. Schiller, J. Gross, J. Mueller, and W. Hunter, "A Total Knee Arthroplasty Prosthesis Capable of Remote Patient Monitoring," *Orthopaedic Proceedings*, Jun. 2021.

[32] L. Wang and D. J. Beebe, "A silicon-based shear force sensor: development and characterization," *Sensors and Actuators A: Physical*, vol. 84, no. 1, pp. 33–44, Aug. 2000.

[33] L. Beccai, S. Roccella, A. Arena, F. Valvo, P. Valdastri, A. Menciassi, M. C. Carrozza, and P. Dario, "Design and fabrication of a hybrid silicon three-axial force sensor for biomechanical applications," *Sensors and Actuators A: Physical*, vol. 120, no. 2, pp. 370–382, May 2005.

[34] A. Tibrewala, A. Phataralaoha, and S. Büttgenbach, "Analysis of full and cross-shaped boss membranes with piezoresistors in transversal strain configuration," *Journal of Micromechanics and Microengineering*, vol. 18, no. 5, p. 055001, May 2008.

[35] V. Nesterov and U. Brand, "Modelling and investigation of the mechanical and electrical characteristics of the silicon 3D-boss microprobe for force and deflection measurements," *Journal of Micromechanics and Microengineering*, vol. 16, no. 7, p. 1116, Apr. 2006.

[36] Followknee project website. https://followknee.com. [Online; accessed 2023-01-13].

[37] "ISO 14879-1 (2001). implants for surgery-total knee-joint prostheses—part 1: Determination of endurance properties of knee tibial trays," International Organization for Standardization, Geneva, CH, Standard, 2001.

[38] W. S. McCulloch and W. Pitts, "A logical calculus of the ideas immanent in nervous activity," *The bulletin of mathematical biophysics*, vol. 5, no. 4, pp. 115–133, Dec. 1943.

[39] K. Hornik, M. Stinchcombe, and H. White, "Multilayer feedforward networks are universal approximators," *Neural Networks*, vol. 2, no. 5, pp. 359–366, Jan. 1989.

[40] K. He, X. Zhang, S. Ren, and J. Sun, "Deep Residual Learning for Image Recognition," in *2016 IEEE Conference on Computer Vision and Pattern Recognition (CVPR)*, Jun. 2016, pp. 770–778, iSSN: 1063-6919.

[41] B. Heinlein, A. Rohlmann, F. Graichen, and G. Bergmann, "Accuracy of an instrumented total knee arthroplasty for six-component in vivo load measurements," Chicago, 2006, p. 605.